(Received 3 July 2025, Accepted 15 October 2025, Scheduled 26 October 2025)

Improved Active-Disturbance Rejection Cascade Control of PMSM Based on New Fast Super-Twisting Non-Singular Terminal Sliding Mode Control Law

Junqin Liu[1,*], Zhentong Wang[1], Haicheng Zhong[1], Feng Deng[1], Kaihui Zhao[2], and Xiangfei Li[2]

[1] *National Key Laboratory of Power Grid Disaster Prevention and Mitigation, College of Electrical and Information Engineering Changsha University of Science and Technology, Changsha 410114, Hunan, China*
[2] *College of Transportation and Electrical Engineering, Hunan University of Technology, Zhuzhou 412007, China*

ABSTRACT: To enhance the disturbance rejection capability and robust stability of PMSM under time-varying disturbance, an improved super-twisting higher-order sliding mode active disturbance rejection cascade control strategy is proposed. Firstly, a second-order mathematical model of the PMSM speed-current dual-loop system is established. Secondly, to address the oscillation issues caused by differentiation of reference speed in conventional linear error feedback control, a composite sliding mode error feedback control law is designed by integrating the fast super-twisting (FST) algorithm and the new fast non-singular terminal sliding mode control (NFNTSMC) method. The control law effectively suppresses system chattering and improves dynamic response. Meanwhile, an improved extended state observer (IESO) is constructed based on deviation control theory, which enhances real-time compensation of the cascade controller by optimizing convergence speed and disturbance estimation accuracy. Finally, hardware-in-the-loop (HIL) simulation results on an RT-LAB platform demonstrate that the proposed method outperforms traditional strategies in both dynamic performance and disturbance rejection, providing a viable solution for high-performance PMSM drive applications.

1. INTRODUCTION

Permanent magnet synchronous motor (PMSM) has been widely adopted in industrial applications due to its excellent power density, compact structural design, and simplified mechanical construction [1, 2]. In traction control systems for electric trains, proportional-integral (PI) control has long been the mainstream solution owing to its simplicity in implementation and technological maturity. However, PMSM is inherently a strongly nonlinear, time-varying system that is highly susceptible to various unmodeled dynamics and random disturbances [3, 4]. PI controllers suffer from intrinsic drawbacks such as integral saturation and inadequate disturbance rejection capability, which often results in performance degradation under dynamic conditions [5, 6]. To improve the control performance of PMSM speed regulation systems, a variety of advanced control strategies have been introduced in recent years [7]. Among them, Sliding Mode Control (SMC) [8] and Active Disturbance Rejection Control (ADRC) [9–11] have gained significant attention. SMC simplifies controller design through order-reduction compensation and ensures that the system trajectory quickly reaches and remains on the sliding surface in finite time [12, 13]. ADRC estimates and compensates disturbances actively, offering superior dynamic response and robustness against both internal uncertainties and external disturbances. These control strategies have demonstrated the ability to achieve fast system response and high-precision tracking, making them prominent directions in modern control theory [14].

Ref. [15] proposed a cascaded control structure combining ADRC and SMC for vehicular opto-electronic tracking platforms. This method effectively enhances tracking performance, resulting in a system with fast response, minimal overshoot, high positional tracking accuracy, strong disturbance rejection, and improved robustness.

To improve the dynamic response and disturbance suppression capabilities of motor drives, Ref. [16] introduced an adaptive ADRC-based speed control strategy. This strategy comprises two key components: a Weighted Hybrid ADRC (HADRC) for suppressing aperiodic disturbances, which provides rapid response and robust steady-state performance and a Feedback Adaptive Resonant Controller (FARC) that offers fast identification and strong robustness against periodic disturbances, while also demonstrating high immunity to measurement noise. Ref. [17] proposed an SMC-based ADRC torque distribution strategy for switched reluctance motors, effectively reducing torque ripple during motor startup. Ref. [18] presented a sliding-mode ADRC method tailored to generator systems, which enabled rapid convergence without overshoot and significantly enhanced disturbance rejection and system robustness.

In contrast to the methods in [17] and [18], which utilize first-order sliding mode control to improve the ADRC controller

* Corresponding author: Junqin Liu (ljq2321925777@163.com).

and to further improve the anti-interference ability and robustness of PMSM, this paper proposes a cascaded ADRC strategy based on FST-NFNTSMC. Firstly, a second-order mathematical model of the PMSM speed-current dual-loop system is established to capture the compound dynamics. Then, to address the oscillation problem caused by differentiating the speed reference signal in traditional linear error feedback control, a composite sliding mode error feedback control law is designed by integrating FST algorithm with NFNTSM control method. In addition, IESO is developed based on deviation control theory to enhance the convergence rate and disturbance estimation accuracy. IESO provides real-time compensation to the cascaded controller, thereby significantly improving the disturbance rejection and robustness of the closed-loop PMSM system. Finally, real-time hardware-in-the-loop (HIL) experiments are conducted to verify the effectiveness and superiority of the proposed composite control algorithm.

2. MATHEMATICAL MODEL OF PMSM

Neglecting all losses, the mathematical model of PMSM can be expressed as follows [19]:

$$\begin{cases} u_d = R_s i_d + L_d \dfrac{di_d}{dt} - \omega_e L_q i_q \\ u_q = R_s i_q + L_q \dfrac{di_q}{dt} + \omega_e \left(L_d i_d + \psi_f\right) \\ T_e = \dfrac{3}{2} n_p \left[\psi_f + \left(L_d - L_q\right) i_d\right] i_q \end{cases} \tag{1}$$

where i_d and i_q denote d-q-axis components of the stator current, respectively; u_d and u_q represent d-q-axis components of the stator voltage; L_d and L_q are the stator inductances; ψ_f is the magnet flux; R_s is the stator resistance; ω_e represents the electrical angular velocity.

Considering the effects of electromagnetic parameter perturbations, the mathematical model of the PMSM can be expressed as:

$$\begin{cases} u_d = R_s i_d + \dfrac{d\psi_d}{dt} - \omega_e \psi_q + \Delta u_d \\ u_q = R_s i_q + \dfrac{d\psi_q}{dt} + \omega_e \psi_d + \Delta u_q \\ T_e = \dfrac{3}{2} n_p \left[\psi_f + (L_d - L_q) i_d\right] i_q + \Delta T_e \end{cases} \tag{2}$$

where Δu_d and Δu_q represent the d-q-axis voltage disturbance; T_e is the electromagnetic torque generated; n_p is the number of pole pairs; ΔT_e is the perturbation in the output electromagnetic torque.

Under ideal conditions, the mechanical motion equation of PMSM is given by:

$$\frac{d\omega_e}{dt} = \frac{n_p}{J} \left(T_e - T_L - B\omega_m\right) \tag{3}$$

where T_L is the load torque; J is the moment of inertia; B is the damping coefficient; ω_m is the mechanical angular velocity of the motor.

3. MATHEMATICAL MODEL OF ADRC

3.1. Mathematical Model of PMSM Speed-Current Cascade Control Loops

The second-order nonlinear system model can be expressed as:

$$\ddot{y} = g(y) + au \tag{4}$$

where $y \in \Re$ represents the system state variables; y and u denote the system output and control input, respectively; $g : \Re \to \Re$ is an unknown nonlinear bounded function that satisfies the Lipschitz condition and depends solely on y; $a \in \Re$ is an unknown gain constant to be determined.

For surface-mounted permanent magnet synchronous motor (SPMSM), using $i_d = 0$ control scheme, Eq. (2) and Eq. (3) can be simplified as follows:

$$\begin{cases} \dot{i}_q = -\frac{R_s}{L_s} i_q - \dfrac{\omega_e \psi_f}{L_s} + \frac{u_q - \Delta u_q}{L_s} \\ \dot{\omega}_e = \dfrac{\left(\frac{3}{2} n_p \psi_f i_q - T_L - \Delta T_e\right)}{J} - \dfrac{B\omega_m}{J} \end{cases} \tag{5}$$

From Eq. (5), the state equation of the composite loop can be expressed as:

$$\ddot{\omega}_e = \begin{bmatrix} \dfrac{3n_p\psi_f}{2JL_s} u_q - \dfrac{\dot{T}_L}{J} - \dfrac{\Delta T_e}{J} - \dfrac{\dot{T}_L}{J} \\ -\dfrac{3n_p\psi_f \left(R_s i_q + n_p \omega_m \psi_f + \Delta u_q\right)}{2JL_s} \end{bmatrix} \tag{6}$$

The PMSM speed-current composite loop mathematical model described by Eq. (6) is given as follows:

$$\ddot{\omega}_e = a u_q + F \tag{7}$$

where a is the parameter to be designed, and F is the total disturbance of the motor composite loop.

3.2. Design of the Traditional ADRC Based on ESO

Defining $\omega_m = x_1$, the state-space representation of the second-order composite loop can be expressed as follows:

$$\begin{cases} \dot{x}_1 = x_2 \\ \dot{x}_2 = a u_q + F \\ y = x_1 \end{cases} \tag{8}$$

The tracking differentiator (TD) is designed as follows [18]:

$$\begin{cases} \dot{n}_1 = n_2 \\ \dot{n}_2 = -1.76\gamma n_2 - \gamma^2 \left(n_1 - \omega_m^*\right) \end{cases} \tag{9}$$

where n_1 and n_2 denote the tracking signal, and γ is the velocity factor.

Assuming that the total F is differentiable, it can be expanded as a new state variable based on Eq. (8). The extended state-space representation of the motor composite loop system is expressed as follows:

$$\begin{cases} \dot{x}_1 = x_2 \\ \dot{x}_2 = x_3 + a u_q \\ \dot{x}_3 = \dot{F} \\ y = x_1 \end{cases} \tag{10}$$

Based on Eq. (10), the third-order Linear Extended State Observer (LESO) model is constructed as follows:

$$\begin{cases} e = z_1 - y \\ \dot{z}_1 = z_2 - \lambda_1 e \\ \dot{z}_2 = z_3 - \lambda_2 e + a u_q \\ \dot{z}_3 = -\lambda_3 e \end{cases} \tag{11}$$

where z_1, z_2, and z_3 represent the estimated values of the motor speed, its derivative, and the total disturbance, respectively; λ_1, λ_2, and λ_3 are the error correction gains. The gains can be chosen as follows:

$$\begin{cases} \lambda_1 = 3\nu \\ \lambda_2 = 3\nu^2 \\ \lambda_3 = \nu^3 \end{cases} \tag{12}$$

where ν denotes the LESO bandwidth. Under this condition, the Hurwitz criterion is satisfied, ensuring stable convergence of the motor state variables within the ESO.

According to Eq. (11), the ESO follows the sequence of tracking z_i to x_i. In the control of variables z_1, z_2, and z_3, when the value of e_1 is small, variables z_2 and z_3 are difficult to observe accurately, making this tracking sequence prone to causing regulation failure in the drive system. To improve the observation accuracy of variables z_2 and z_3, the ESO typically requires error correction gains λ_2 and λ_3 to be designed as large gain coefficients; however, choosing a too large value for λ_3 will degrade the transient performance of the ESO.

4. DESIGN OF IADRC-IESO BASED ON FST-FNFTSM CONTROL LAW

4.1. Designing the IESO for IADRC

To address this issue, an Improved Extended State Observer (IESO) model for the PMSM is established [20], and Eq. (11) is modified as follows:

$$\begin{cases} z_1 = x_1 + e \\ z_2 = z_1 + \lambda_1 e \\ z_3 = \dot{z}_2 + \lambda_2 e - a u_q \end{cases} \tag{13}$$

From Eq. (13), the error dynamics can be described as follows:

$$\begin{cases} z_1 - x_1 = e \\ z_2 - x_2 = \dot{e} + \lambda_1 e \\ z_3 - x_3 = \ddot{e} + \lambda_1 \dot{e} + \lambda_2 \left(\dot{e} + \lambda_1 e\right) \end{cases} \tag{14}$$

Based on Eq. (14), the IESO model of the PMSM can be described as follows:

$$\begin{cases} e = z_1 - x_1 \\ \dot{z}_1 = z_2 - \lambda_1 e \\ \dot{z}_2 = z_3 - \lambda_2 [\dot{e} + \lambda_1 e] + a u_q \\ \dot{z}_3 = -\lambda_3 \left[\ddot{e} + \lambda_1 \dot{e} + \lambda_2 \left(\dot{e} + \lambda_1 e\right)\right] \end{cases} \tag{15}$$

4.2. Design of the FST-NFNTSM Control Law

The state error equation is defined as follows:

$$\begin{cases} e_1 = x_1 - n_1 \\ e_2 = \dot{e}_1 = x_2 - n_2 \end{cases} \tag{16}$$

The new fast non-singular terminal sliding mode (NFNTSM) surface is selected as [21]:

$$s = e_2 + l_1 e_1 + l_2 e^{-gt} e_1^{1-2b} \tag{17}$$

where l_1 and l_2 are positive constants $0 < b < 1$.

To reduce sliding mode chattering and improve the smoothness of the motor output signal, a segmented error feedback control law is designed as follows:

$$u_q = u_1 + u_2 \tag{18}$$

where u_1 and u_2 represent the equivalent control term and nonlinear control term, respectively.

Taking the derivative of Eq. (17):

$$\dot{s} = \dot{e}_2 + l_1 \dot{e}_1 + l_2 e^{-gt} e_1^{-2b} \left[(1-2b)\dot{e}_1 - g e_1\right] \tag{19}$$

In accordance with Eq. (8), Eq. (18), and Eq. (19), the nonlinear control term u_1 can be expressed as follows:

$$u_1 = \frac{1}{a}\left[-l_1 e_2 + l_2 e^{-gt} e_1^{-2b} \cdot \left(g e_1 - (1-2b)\, e_2\right) - F + \dot{n}_2\right] \tag{20}$$

To ensure that the state variables of the control system enter the sliding mode, FST control law [22] is introduced as follows:

$$\begin{cases} \dot{s} = -k_1 |s|^{\frac{1}{2}} \operatorname{sgn}(s) - k_2 s + h + F \\ \dot{h} = -k_3 \operatorname{sgn}(s) \end{cases} \tag{21}$$

where k_1, k_2, and k_3 are all positive constants.

By combining Eq. (18) and Eq. (21), the expression for the equivalent control term u_2 can be obtained as:

$$u_2 = \frac{-k_1 |s|^{\frac{1}{2}} \operatorname{sgn}(s) - k_2 s - \int k_3 \operatorname{sgn}(s) dt + F}{a} \tag{22}$$

While $e^{-gt} = 0$, the fast terminal sliding surface is reduced to a linear sliding surface. By appropriately selecting function g, the proposed sliding surface can exhibit characteristics of both terminal and linear sliding modes.

Theorem 1: For a nonlinear, strongly coupled, and multivariable PMSM system, if the dynamic sliding surface is designed as in Eq. (17), and the fast super-twisting sliding mode control law in Eq. (21) is adopted, then while $2bl_1 - g > 0$, the tracking error will converge to 0. The convergence time T_s can be estimated as:

$$T_s \le \frac{\ln\left(1 + \frac{e^{2bl_1 t} V^b(0)}{c}\right)}{2bl_1 - g} \tag{23}$$

Proof 1: Defining the Lyapunov function V as follows:

$$V = \frac{1}{2} e_1^2 \tag{24}$$

According to the equation, letting $\dot{s}=0$:

$$\dot{e}_1 = -l_1 e_1 - l_2 e^{-gt} e_1^{1-2b} \tag{25}$$

The derivative of Eq. (24) can be obtained as:

$$\begin{aligned}\dot{V} &= e_1\dot{e}_1 = e_1\left(-l_1 e_1 - l_2 e^{-gt} e_1^{1-2b}\right)\\ &= -l_1 e_1^2 - l_2 e^{-gt} e_1^{2(1-b)}\\ &= -2l_1 V - 2^{1-b} l_2 e^{-gt} V^{1-b} \le 0\end{aligned} \tag{26}$$

According to the Lyapunov stability criterion, it can be concluded that the system state variables will converge to zero within a finite time. To further derive the convergence time of the system states, both sides of Eq. (26) are multiplied by bV^{b-1}:

$$bV^{b-1}\frac{dV_1}{dt} \le -2bl_1 V^b - 2^{1-b} bl_1 e^{-gt} \tag{27}$$

$$\frac{dV^b}{dt} + 2bl_1 V^b \le -2^{1-b} bl_2 e^{-gt} \tag{28}$$

Multiplying both sides of Eq. (28) by $e^{2bl_1 t}$:

$$e^{2bl_1 t}\left(\frac{dV^b}{dt} + 2bl_1 V^b\right) \le -2^{1-b} bl_2 e^{(2bl_1-g)t} \tag{29}$$

$$\frac{d\left(e^{2bl_1 t}V^b\right)}{dt} \le -2^{1-b} bl_2 e^{(2bl_1-g)t} \tag{30}$$

Integrating both sides of Eq. (30) from 0 to T_s, and letting $V(T_s)=0$:

$$-e^{2bl_1 t}V^b(0) \le \frac{-2^{1-b}bl_2}{2bl_1-g}\left(e^{(2bl_1-g)T_s}-1\right) \tag{31}$$

Letting $c=\frac{2^{1-b}bl_2}{2bl_1-g}>0$, Eq. (31) can be rewritten as:

$$T_s \le \frac{\ln\left(1+\frac{e^{2bl_1 t}V^b(0)}{c}\right)}{2bl_1-g} \tag{32}$$

Proof 2: Selecting Lyapunov function $V_1(x)$ as

$$\begin{aligned}V_1(x) &= 2k_3|s| + \frac{1}{2}h^2 + \frac{1}{2}\dot{s}^2\\ &= \frac{1}{2}\begin{bmatrix}(4k_3+k_1^2)|s|^{\frac{1}{2}}\operatorname{sgn}(s) - k_1k_2 s - k_1 h\\ -k_1k_2|s|^{\frac{1}{2}}\operatorname{sgn}(s) + k_2^2 s + k_2 h\\ -k_1|s|^{\frac{1}{2}}\operatorname{sgn}(s) + k_2 s + 2h\end{bmatrix}^{\mathrm{T}}\\ &\quad\begin{bmatrix}|s|^{\frac{1}{2}}\operatorname{sgn}(s)\\ s\\ h\end{bmatrix}\end{aligned} \tag{33}$$

Eq. (33) can be simplified to

$$V_1 = \boldsymbol{\zeta}^{\mathrm{T}}\mathbf{Q}\boldsymbol{\zeta} \tag{34}$$

where $\mathbf{Q} = \frac{1}{2}\begin{bmatrix}(4k_3+k_1^2) & -k_1k_2 & -k_1\\ -k_1k_2 & k_2^2 & k_2\\ -k_1 & k_2 & 2\end{bmatrix}$, $\boldsymbol{\zeta} = \begin{bmatrix}|s|^{\frac{1}{2}}\operatorname{sgn}(s)\\ s\\ h\end{bmatrix}$.

In Eq. (34), $|\mathbf{Q}_1|>0$, $|\mathbf{Q}_2|>0$, and $|\mathbf{Q}_3|>0$ represent the determinants of the first-order, second-order, and third-order master forms, respectively. The matrix $\mathbf{Q}$ is positive definite, and V_1 is a positive definite, continuous function. Applying the chain rule to relate $d|x|/dt = \dot{x}\operatorname{sgn}(x)$ and $\dot{V}_1$, the derivative of $\boldsymbol{\zeta}$ is obtained as follows:

$$\begin{aligned}\dot{\boldsymbol{\zeta}} &= \begin{bmatrix}|s|^{1/2}\operatorname{sgn}(s) & s & h\end{bmatrix}^{\mathrm{T}}\\ &= \frac{1}{2|s|^{1/2}}\begin{bmatrix}-k_1 & k_2 & 1\\ 0 & 0 & 0\\ -2k_3 & 0 & 0\end{bmatrix}\begin{bmatrix}|s|^{\frac{1}{2}}\operatorname{sgn}(s)\\ s\\ h\end{bmatrix}\\ &\quad+\begin{bmatrix}0 & 0 & 0\\ -k_1 & k_2 & 1\\ 0 & 0 & 0\end{bmatrix}\boldsymbol{\zeta}+\begin{bmatrix}0\\ 0\\ \dot{F}\end{bmatrix}\\ &= \frac{1}{|s|^{1/2}}\mathbf{W}\boldsymbol{\zeta} + \mathbf{L}\boldsymbol{\zeta} + \boldsymbol{\upsilon}\end{aligned} \tag{35}$$

where $\mathbf{W} = \frac{1}{2}\begin{bmatrix}-k_1 & k_2 & 1\\ 0 & 0 & 0\\ -2k_3 & 0 & 0\end{bmatrix}$, $\mathbf{L} = \begin{bmatrix}0 & 0 & 0\\ -k_1 & k_2 & 1\\ 0 & 0 & 0\end{bmatrix}$, $\boldsymbol{\upsilon} = \begin{bmatrix}0\\ 0\\ \dot{F}\end{bmatrix}$.

Taking the derivative of $\dot{V}_1$:

$$\begin{aligned}\dot{V}_1 &= \dot{\boldsymbol{\zeta}}^{\mathrm{T}}\mathbf{Q}\boldsymbol{\zeta} + \boldsymbol{\zeta}^{\mathrm{T}}\mathbf{Q}\dot{\boldsymbol{\zeta}} = -\frac{1}{|s|^{1/2}}\boldsymbol{\zeta}^{\mathrm{T}}\mathbf{P}_1\boldsymbol{\zeta} - \boldsymbol{\zeta}^{\mathrm{T}}\mathbf{P}_2\boldsymbol{\zeta} + \dot{F}\boldsymbol{\rho}^{\mathrm{T}}\boldsymbol{\zeta}\\ &\le -\frac{1}{|s|^{1/2}}\boldsymbol{\zeta}^{\mathrm{T}}\mathbf{P}_1\boldsymbol{\zeta} - \boldsymbol{\zeta}^{\mathrm{T}}\mathbf{P}_2\boldsymbol{\zeta} + \delta\boldsymbol{\rho}^{\mathrm{T}}\boldsymbol{\zeta}\end{aligned} \tag{36}$$

where $\boldsymbol{\rho} = \begin{bmatrix}-k_1\\ k_2\\ 2\end{bmatrix}$,

$$P_1 = \frac{1}{2}\begin{bmatrix}2k_1k_3+k_1^3 & (k_1^2+k_3)k_2 & k_1^2\\ (k_1^2+k_3)k_2 & -k_1k_2^2 & -k_1k_2\\ k_1^2 & -k_1k_2 & -k_1\end{bmatrix},$$

$$P_2 = \begin{bmatrix}k_1^2k_2 & -k_1k_2^2 & -k_1k_2\\ -k_1k_2^2 & k_2^3 & k_2^2\\ -k_1k_2 & k_2^2 & k_2\end{bmatrix},\quad \dot{F}\le\delta.$$

The boundary of $\dot{F}$ is

$$\dot{\mathbf{F}}\boldsymbol{\rho}^{\mathrm{T}}\boldsymbol{\zeta} = \frac{1}{|s|^{1/2}}\boldsymbol{\zeta}^{\mathrm{T}}\mathbf{M}_1\boldsymbol{\zeta} + \boldsymbol{\zeta}^{\mathrm{T}}\mathbf{M}_2\boldsymbol{\zeta} \tag{37}$$

TABLE 1. The parameters of PMSM.

Motor Parameters	Units	Values
flux linkage ψ_f	Wb	0.171
Stator q-axis inductance L_q	H	0.00334
Stator d-axis inductance L_d	H	0.00334
Stator resistance R_s	Ω	1.9
Number of pole pairs n_p	pair	4
Moment of inertia J	kg·m^2	0.001469

where $\mathbf{M}_1 = \begin{bmatrix} -k_1\dot{F}\text{sgn}(s) & 0 & \dot{F}\text{sgn}(s) \\ 0 & k_2\dot{F} & 0 \\ \dot{F}\text{sgn}(s) & 0 & 0 \end{bmatrix}$, $\mathbf{M}_2 = \begin{bmatrix} -k_2\dot{F}\text{sgn}(s) & 0 & 0 \\ 0 & 0 & 0 \\ 0 & 0 & 0 \end{bmatrix}$.

Substituting Eq. (37) into Eq. (36):

$$\begin{aligned}\dot{V}_1 &= -\frac{1}{|s|^{1/2}}\boldsymbol{\zeta}^{\mathrm{T}}\mathbf{P}_1\boldsymbol{\zeta} - \boldsymbol{\zeta}^{\mathrm{T}}\mathbf{P}_2\boldsymbol{\zeta} + \frac{1}{|s|^{1/2}}\boldsymbol{\zeta}^{\mathrm{T}}\mathbf{M}_1\boldsymbol{\zeta} + \boldsymbol{\zeta}^{\mathrm{T}}\mathbf{M}_2\boldsymbol{\zeta} \\ &= -\frac{1}{|s|^{1/2}}\boldsymbol{\zeta}^{\mathrm{T}}\left(\mathbf{P}_1 - \mathbf{M}_1\right)\boldsymbol{\zeta} - \boldsymbol{\zeta}^{\mathrm{T}}\left(\mathbf{P}_2 - \mathbf{M}_2\right)\boldsymbol{\zeta} \end{aligned} \tag{38}$$

From Eq. (38), while $\mathbf{P}_1 - \mathbf{M} > 0$ and $\mathbf{P}_2 - \mathbf{M}_2 > 0$, $\dot{V}_1 < 0$. The necessary and sufficient condition for $\mathbf{P}_1 - \mathbf{M} > 0$ and $\mathbf{P}_2 - \mathbf{M}_2 > 0$ is

$$\begin{cases} k_1^2 + 2k_3 + 2\dot{F}\text{sgn}(s) > 0 \\ k_2^2(k_3^2 - 2k_1^2\dot{F}\text{sgn}(s)) > 0 \\ k_2^2(9k_1^2 + 8k_3 + 28\dot{F}\text{sgn}(s) + 20\dot{F}^2/k_1^2) < 0 \\ 2k_1^2 + \dot{F}\text{sgn}(s) > 0 \\ k_1^2 + \dot{F}\text{sgn}(s) - k_1^2k_2 > 0 \end{cases} \tag{39}$$

From Eq. (39), Eq. (40) can be rewritten as:

$$\lambda_{\min}(\mathbf{Q})\|\zeta\|^2 < V_1 < \lambda_{\max}(\mathbf{Q})\|\zeta\|^2 \tag{40}$$

From the quadratic standard inequality, we can see that

$$|s|^{1/2} \le \|\boldsymbol{\zeta}\| \le V_1^{1/2}/\lambda_{\min}^{1/2}(\mathbf{Q}) \tag{41}$$

where $\|\boldsymbol{\zeta}\| = \sqrt{|s| + |s|^2 + |h|^2}$.

In summary, it can be concluded that

$$\begin{aligned}\dot{V}_1 &= -\frac{1}{|s|^{1/2}}\boldsymbol{\zeta}^{\mathrm{T}}\left(\mathbf{P}_1 - \mathbf{M}_1\right)\boldsymbol{\zeta} - \boldsymbol{\zeta}^{\mathrm{T}}\left(\mathbf{P}_2 - \mathbf{M}_2\right)\boldsymbol{\zeta} \\ &\le -\mu_1 V_1^{1/2} - \mu_2 V_1^{1/2} \le 0 \end{aligned} \tag{42}$$

where $\mu_1 = \frac{\lambda_{\min}^{1/2}(\mathbf{Q})\delta(\mathbf{P}_1-\mathbf{M}_1)}{\lambda_{\max}^{1/2}(\mathbf{Q})}$, $\mu_2 = \frac{\lambda_{\min}^{1/2}(\mathbf{P}_2-\mathbf{M}_2)}{\lambda_{\max}(\mathbf{Q})}$, $\lambda_{\min}(\mathbf{Q})$ and $\lambda_{\max}(\mathbf{Q})$ are the minimum and maximum eigenvalues of $\mathbf{Q}$, respectively. For Eq. (42), the system state error will converge to zero in finite time.

TABLE 2. The experimental conditions.

Time	Perturbation	Perturbation Range
0 s	n/r/min	0→1000
0.1 s	T_L/N·m	0→10
0.2 s	n/r/min	1000→2000
0.3 s	ψ_f/Wb	0.171→0.14
0.4 s	n/r/min	2000→1000
0.5 s	R_s/Ω	1.9→2.9
0.6 s	L_s/H	0.00334→0.0047

This paper uses $H(s)$ instead of sgn(s), and $H(s)$ is expressed as:

$$H(s) = \frac{s}{|s| + \sigma} \tag{43}$$

where $\sigma > 0$.

5. ANALYSIS OF SIMULATION AND EXPERIMENT RESULTS

Table 1 shows the parameters of PMSM. Fig. 1 displays the control block diagram of PMSM. To verify the disturbance rejection performance of the proposed control strategy, comparative experiments are conducted under motor parameter perturbation conditions as specified in Table 2. Fig. 2 presents the simulation comparison among PI, conventional ADRC, and Improved ADRC (IADRC).

Remark 1: *a is rectified by $a = 3n_p\psi_f/2JL_s$ in the system; l_1 and l_2 are the gain coefficients for the system state variables and directly influence the dynamic quality of the sliding surface. To ensure finite-time convergence of the sliding surface and optimize control performance, the parameter tuning process adheres to the following procedure: Firstly, a preset baseline value is established for the parameters based on theoretical analysis or empirical knowledge to guarantee global stability of the system. Subsequently, each parameter is fine-tuned progressively to optimize the transient response and suppress chattering; k_1, k_2, and k_3, as the key parameters of the fast super-twisting (FST) control law, directly determine the dynamic quality of the convergence process of the sliding mode variable structure. To optimize system performance, this study adopts a speed-comparison-based tuning method: by analyzing the system's response characteristics under two speed settings of 1000 r/min and 2000 r/min, and considering the observed chattering level, these parameters are fine-tuned accordingly to achieve an optimal balance between convergence speed and steady-state accuracy. σ is primarily employed to suppress high-frequency chattering in the sliding mode motion, representing a form of local performance optimization. Its tuning is based on the speed waveform of the motor during steady-state operation. By observing and quantifying the amplitude of speed fluctuations, this parameter is adjusted accordingly to maximize the smoothness of the control output while preserving dynamic performance, $\sigma > 0$.*

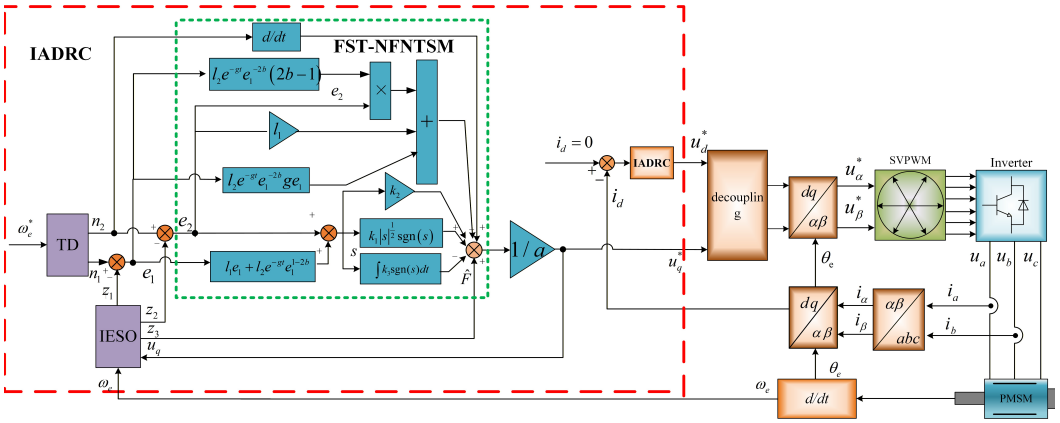

FIGURE 1. The control block diagram of the PMSM system.

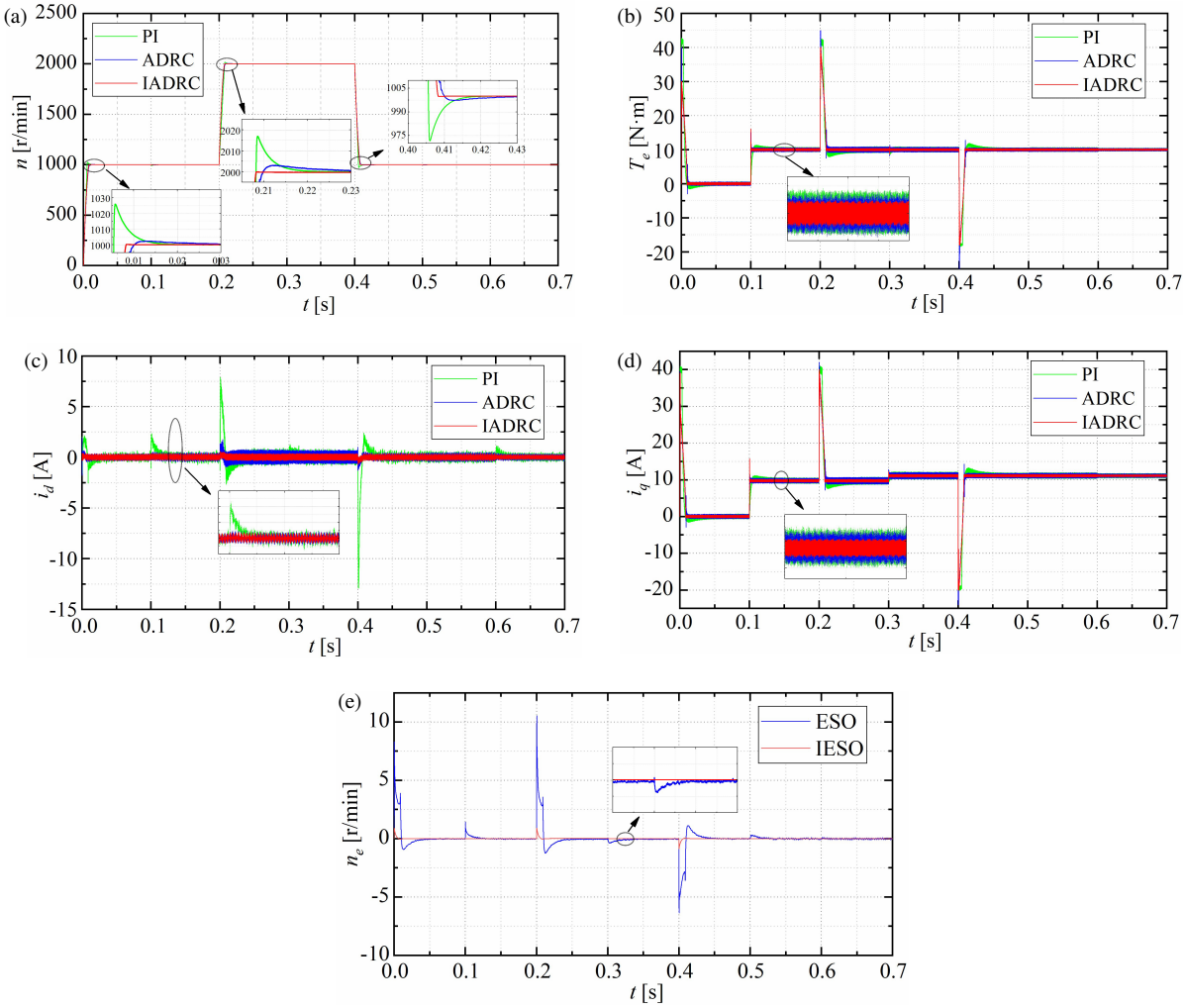

FIGURE 2. Simulation results of PI, ADRC, and IADRC. (a) Simulation results of n. (b) Simulation results of T_e. (c) Simulation results of i_d. (d) Simulation results of i_q. (e) The error of n.

5.1. Analysis of Simulation Results

Figure 2(a) illustrates the speed response characteristics under different control strategies. When the speed steps from 0 r/min to 1000 r/min, the IADRC achieves steady speed within 0.008 s, whereas the PI and conventional ADRC require 0.02 s and 0.015 s, respectively. At 0.2 s, when the speed changes from 1000 r/min to 2000 r/min, the IADRC continues to demonstrate superior dynamic performance, completing speed tracking by 0.21 s, compared to 0.22 s and 0.23 s for the PI and conventional ADRC, respectively. Moreover, under the parameter perturbations, both PI and conventional ADRC exhibit noticeable speed fluctuations and overshoot, with longer recovery

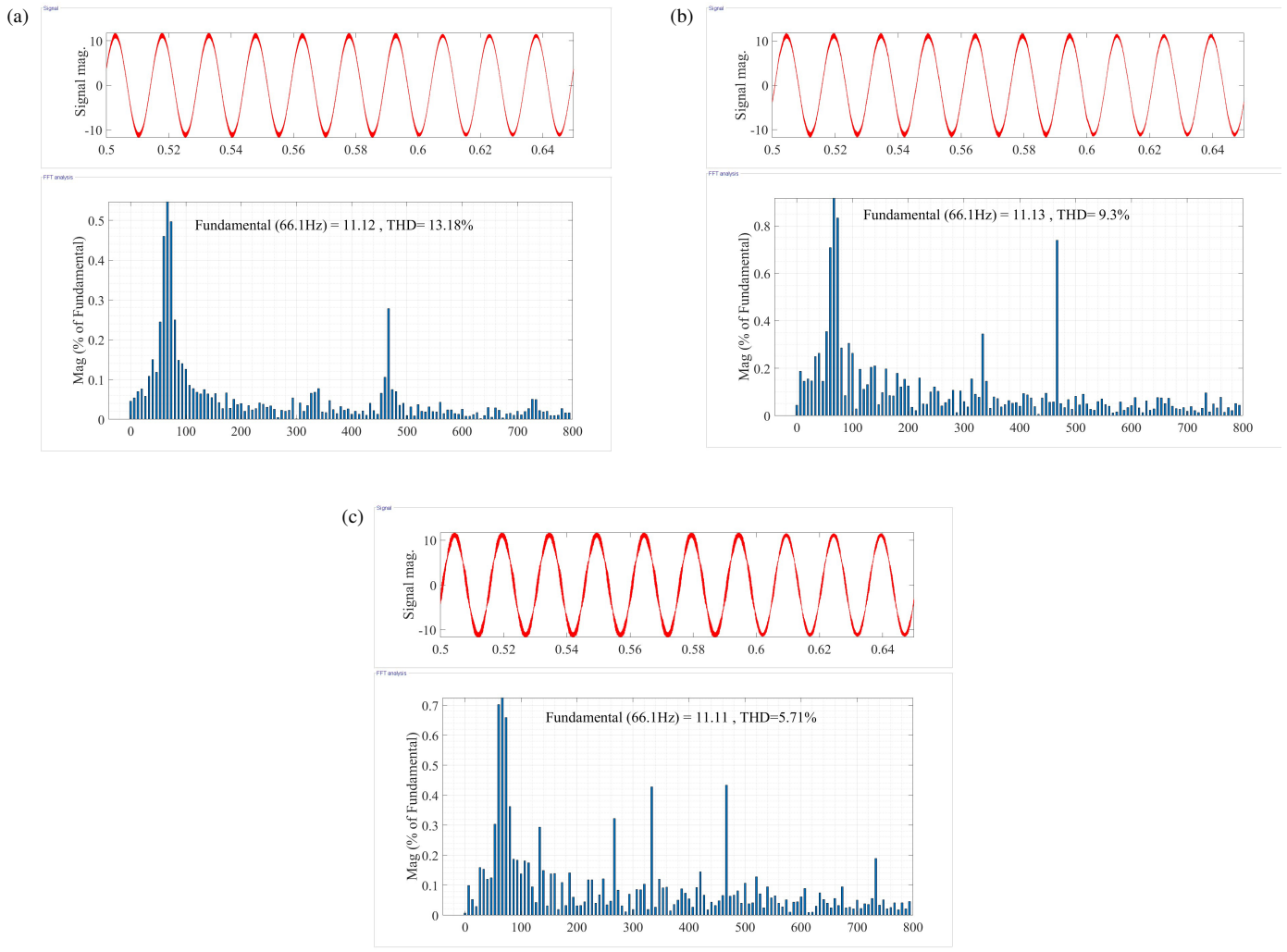

FIGURE 3. The THD analysis of i_a for PI, ADRC, and IADRC. (a) PI. (b) ADRC. (c) IADRC.

times. In contrast, the IADRC rapidly and accurately tracks the given speed, achieving significantly better steady-state accuracy than traditional methods.

Figures 2(b)–(d) compare the torque and d-q axis current waveforms under different control strategies. The results demonstrate that the IADRC yields superior stability in both transient and steady-state processes, with the smallest ripple amplitude.

Figure 2(e) further validates the superiority of the IESO. Compared to the traditional ESO, IESO exhibits faster tracking speed and reduced overshoot under parameter perturbations, while effectively suppressing observer chattering.

Based on the stator phase current total harmonic distortion (THD) spectral analysis shown in Fig. 3, THD values for the PI controller, conventional ADRC, and proposed method are 13.18%, approximately 9.3%, and only 5.71%, respectively. These results indicate that the proposed method significantly reduces high-frequency current harmonics in the motor drive system. Compared to both conventional PI and ADRC, IADRC strategy achieves a smoother speed output, leading to substantially improved harmonic suppression performance and further demonstrating the superior control capability of the proposed approach.

5.2. Analysis of RT-LAB Results

To verify the feasibility and effectiveness of the proposed algorithm, the model of PMSM is constructed using an RT-LAB (HIL) platform. Fig. 4 depicts the RT-LAB (HIL) experimental platform. Fig. 5 presents the RT-LAB experimental results for PI, ADRC, and IADRC.

Based on the simulation results shown in Figs. 2 and 5, the overall performance of PI and ADRC is limited. In contrast, the

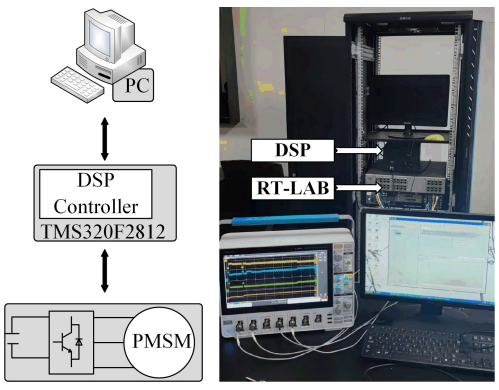

FIGURE 4. The experimental platform of RT-LAB.

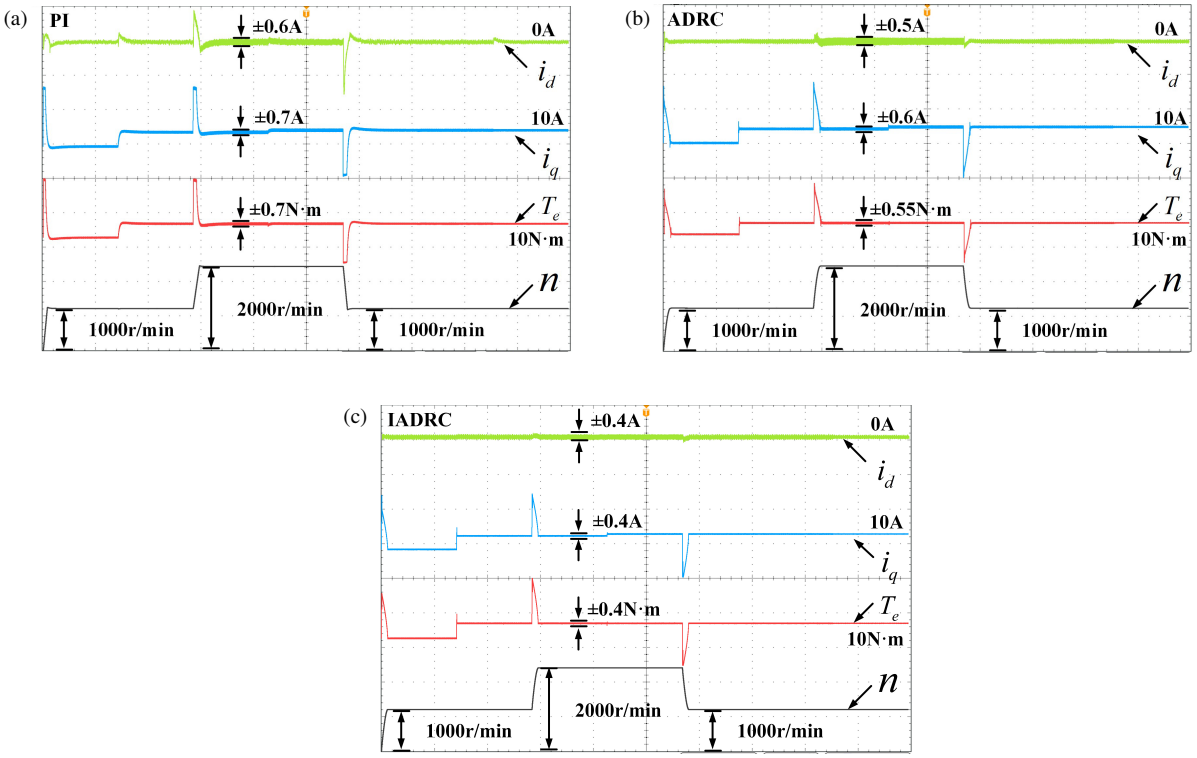

FIGURE 5. The RT-LAB experimental results for PI, ADRC, and IADRC. (a) PI. (b) ADRC. (C) IADRC.

TABLE 3. The comparison of the results for PI, ADRC, and IADRC.

Performances	PI	ADRC	IADRC
Speed Response	0.03	0.02	0.009
Torque Ripple	14.3%	10.9%	8.26%
Speed Error	0.54	0.31	0.21
THD	13.18%	9.3%	5.71%

proposed IADRC method effectively overcomes these shortcomings, enabling the PMSM drive system to achieve high-precision control. Table 3 summarizes the performance comparison among PI, ADRC, and IADRC.

The data in Table 3 collectively demonstrate the superior performance of the proposed method, characterized by rapid and overshoot-free speed tracking, smoother speed output, minimal transient current, and significantly reduced torque ripple, leading to enhanced overall reliability.

6. CONCLUSION

To enhance the disturbance rejection capability and robust stability of PMSM, this paper proposes an IADRC strategy based on FST-NFNTSMC. The proposed approach follows the technical framework below:

(1) A second-order mathematical model of the PMSM speed-current dual-loop system is established. To address the system oscillations caused by the differentiation of the speed reference in traditional linear error feedback control, a novel composite sliding mode error feedback control law is proposed by integrating the FST algorithm with the NFNTSM. The FST-NFNTSM control law effectively suppresses the influence of the second-order derivative of the system speed caused by the Tracking Differentiator (TD), owing to its integration of the advantages of both the Fast Super-Twisting algorithm and Non-singular Terminal Sliding Mode.

(2) IESO is designed based on disturbance rejection theory. It significantly enhances the dynamic convergence speed and effectively strengthens the disturbance rejection capability and robustness of the motor's cascade closed-loop control system.

(3) Finally, the proposed composite control algorithm is experimentally validated using an RT-LAB platform. The test results demonstrate that the control strategy exhibits significant improvements in dynamic performance and disturbance rejection capability, confirming the effectiveness and superiority of the proposed method.

ACKNOWLEDGEMENT

This work was supported by the Natural Science Foundation of Hunan Province Grant 2023JJ50193, and the Postgraduate Scientific Research Innovation Project of Hunan Province Grant CX20231107.

REFERENCES

[1] Zhang, B., R. Qi, and H. Lin, "Back-stepping sliding mode control of laser cutting permanent magnet linear servo control system," *Transactions of China Electrotechnical Society*, Vol. 33, No. 3, 642–651, 2018.

[2] Cheng, S., H. Wang, and Y. Jiang, "Improved orthogonal flux corrector-based rotor flux estimation in PMSM sensorless con-

trol," *Progress In Electromagnetics Research Letters*, Vol. 121, 57–63, 2024.

[3] He, Y., K. Zhao, Z. Yi, and Y. Huang, "Improved terminal sliding mode control of PMSM dual-inertia system with acceleration feedback based on finite-time ESO," *Progress In Electromagnetics Research M*, Vol. 134, 21–30, 2025.

[4] Li, X., J. Liu, K. Zhao, Y. Yin, and L. Zou, "Improved nonsingular fast terminal sensor-less sliding mode control of IPMSM considering external disturbance and parameter perturbation," *Progress In Electromagnetics Research B*, Vol. 102, 81–98, 2023.

[5] Wei, H. and L. Wang, "Adaptive fuzzy neural network time-varying sliding mode control for permanent magnet linear synchronous motor," *Transactions of China Electrotechnical Society*, Vol. 37, No. 4, 861–869, 2022.

[6] Wang, D., C. Peng, B. Wang, Z. Feng, and F. Zhang, "Research on a novel interior permanent magnet machine with segmented rotor to mitigate torque ripple and electromagnetic vibration," *Proceedings of the CSEE*, Vol. 42, No. 14, 5289–5299, 2022.

[7] Wang, J., R. Zhou, and J. Liu, "New non-singular fast terminal sliding mode control of permanent magnet synchronous motor based on super-twisting sliding mode observer," *Progress In Electromagnetics Research C*, Vol. 146, 151–162, 2024.

[8] Li, X., J. Liu, K. Zhao, Y. Yin, and L. Zou, "An improved model-free sliding mode control algorithm of super-twisting for SPMSM," *Progress In Electromagnetics Research C*, Vol. 135, 195–210, 2023.

[9] Wang, X., Z. Yang, X. Sun, and S. Zhan, "Research on the control system of bearing-less nduction motor based on improved active disturbance rejection control," *Progress In Electromagnetics Research C*, Vol. 141, 123–132, 2024.

[10] Han, J. Q., "Auto disturbance rejection controller and it's applications," *Control and Decision*, Vol. 13, No. 1, 19–23, 1998.

[11] Kang, E., S. Shi, and S. Li, "Suppression strategy for uncertain current disturbances in PMSM based on frequent adaptive active disturbance rejection controller," *Electric Machines and Control*, Vol. 29, No. 4, 124–134, 2025.

[12] Zhao, K., W. Liu, T. Yin, R. Zhou, and W. Dai, "Model-free sliding mode control for PMSM drive system based on ultra-local model," *Energy Engineering: Journal of the Association of Energy Engineers*, Vol. 119, No. 2, 767–780, 2022.

[13] Wu, Y.-J., J.-X. Zuo, and L.-H. Sun, "Adaptive terminal sliding mode control for hypersonic flight vehicles with strictly lower convex function based nonlinear disturbance observer," *ISA Transactions*, Vol. 71, 215–226, 2017.

[14] Zhao, K. H., W. K. Dai, R. R. Zhou, A. Leng, W. Liu, P. Qiu, G. Huang, and G. Wu, "Novel model-free sliding mode control of permanent magnet synchronous motor based on extended sliding mode disturbance observer," *Proceedings of the CSEE*, Vol. 42, No. 6, 2375–2386, 2022.

[15] Wu, Z., Z. Chen, B. Xu, S. Pang, and F. Lin, "Realization of control algorithm for vehicle optoelectronic tracking platform based on sliding mode control and active disturbance rejection control optimized by differential evolution algorithm," *IEEE Access*, Vol. 11, 60 386–60 397, 2023.

[16] Cheng, Z., L. Li, C. Zhong, J. Wang, X. Bai, and J. Liu, "Adaptive hybrid active disturbance rejection speed control for vehicle PMSM electric propulsion system under uncertain disturbances," *IEEE Transactions on Energy Conversion*, 2025.

[17] Li, Z., H. Chen, Y. Qi, *et al.*, "Torque sharing function control strategy for switched reluctance motor based on active disturbance rejection sliding mode control," *Transactions of China Electrotechnical Society*, Vol. 39, No. 18, 5639–5656, 2024.

[18] Feng, X., P. Huang, Z. Zhang, *et al.*, "Sliding mode active disturbance rejection control of generator sets based on GA fuzzy RBF," *Journal of Instrumentation*, Vol. 44, No. 8, 319–328, 2023.

[19] Guo, X., S. Huang, K. Lu, Y. Peng, H. Wang, and J. Yang, "A fast sliding mode speed controller for PMSM based on new compound reaching law with improved sliding mode observer," *IEEE Transactions on Transportation Electrification*, Vol. 9, No. 2, 2955–2968, 2023.

[20] Sun, D. and Y. Zhang, "Improvement and observation accuracy analysis of linear extended state observer," *Journal of National University of Defense Technology*, Vol. 39, No. 6, 111–117, 2017.

[21] Zhao, K., M. Qiao, Y. Lyu, X. You, C. Zhang, and J. Zheng, "Model-free super-twisting fast integral terminal sliding mode control for PMSM," *Journal of Electronic Measurement and Instrumentation*, Vol. 38, No. 5, 64–74, 2024.

[22] Li, X., Z. Yi, J. Liu, K. Zhao, and L. Zou, "Deep flux weakening of IPMSM based on feedback super-twisting non-singular fast terminal sliding mode control," *Journal of Electronic Measurement and Instrumentation*, Vol. 38, No. 11, 132–145, 2024.